Surface Disturbance Evolution and the Splattering of Turbulent Liquid Jets

Sourav K. Bhunia

John H. Lienhard V

W. M. Rohsenow Heat and Mass Transfer Laboratory, Department of Mechanical Engineering, Massachusetts Institute of Technology, Cambridge, MA 02139

In this study, we investigate the growth of surface disturbances on turbulent liquid jets in air and its relation to the amount of splattering when the jet strikes a target. A laser-based optical technique is used to measure the instantaneous local amplitude of fluctuations on jets produced by fully-turbulent tube nozzles. Measurements were made over the portion of the jet between 0.2 and 45 nozzle diameters downstream of the nozzle. Jets of water, an isopropanol-water mixture, and water with a surfactant were studied. The local rms amplitude of surface disturbances scales with the jet Weber number and the dimensionless distance from the target. The measurements show a nonexponential growth of the rms amplitude as the liquid moves downstream. Power spectra of the disturbance amplitudes show broadband turbulent disturbances to be dominant over any single wavenumber Rayleigh-type instability. The measured rms amplitude of roughness on the jet surface correlates well with the fraction of impinging liquid splattered, as hypothesized in previous models of splattering. A mathematical model of the free-surface/turbulence interaction is also given. The spectrum of surface disturbances is calculated based on the pressure spectrum of isotropic, homogeneous turbulence. Both the theoretical model and the experiments show that the high-wavenumber portion of the spectrum decays as $k^{-19/3}$ owing to the damping effect of capillary forces on the turbulent pressure spectrum that drives surface roughening.

1 Introduction

The disturbances on the free surface of a turbulent liquid jet cause splattering of liquid when the jet strikes a surface and are thus critical to the control of jet impingement cooling and cleaning processes. The rate of surface roughening is also important to absorption in jet systems (Kim and Mills, 1989) and to jet atomization processes. No detailed measurements of the instantaneous amplitudes of these disturbances are available in the literature. Many photographic studies of turbulent jets have been reported (e.g., Hoyt et al., 1974), but photography does not generally provide sufficient temporal resolution for high-frequency time-series analysis or spectral determination. The only time-resolved measurements of the turbulent-disturbance amplitude that the authors have found were by Chen and Davis (1964), who presented a few rms amplitude measurements obtained with an electrical conductivity probe. The accuracy of those data was severely limited by the interference of the instrument with the flow.

In the present work, we use a laser-based optical technique to measure the amplitudes of fluctuations on the free surface of a turbulent jet in air (following Tadrist et al., 1991). This instrument, consisting of a laser light sheet, a photosensor, and lenses, is capable of measuring fluctuations in jet diameter at frequencies up to about 1 MHz. The jets were produced by fully developed turbulent pipe flow issuing from straight tube nozzles.

A key objective of this study is to assess the relationship between jet surface roughness and splattering during jet impingement. In a previous study, we examined the process by which liquid droplets are splattered when a turbulent jet impacts a solid surface normal to its axis (Bhunia and Lienhard, 1994). Splattering was found to occur when disturbances on the jet are carried into the liquid moving along the target, where they are amplified and cause droplets to be ejected. The results of that study showed that spattering increases as the dimensionless jet length increases and as the jet Weber number increases (i.e., as surface tension decreases). Since turbulent roughening of the jet surface is greater for longer jets and for jets of lower surface tension, these trends were credited to an increasingly rough jet surface when the jet reached the target. The present measurements allow a direct test of the correlation between jet surface-roughness and the fraction of incoming liquid that is splattered.

A mathematical model of free-surface response to turbulence is also developed. At modest values of air-side Reynolds number, the free surface deforms in response to turbulent pressure fluctuations in the liquid. Capillary pressure provides the restoring force that balances the turbulent pressure, and this

Contributed by the Fluids Engineering Division for publication in the JOURNAL OF FLUIDS ENGINEERING. Manuscript received by the Fluids Engineering Division September 15, 1993; revised manuscript received May 10, 1994. Associate Technical Editor: M. W. Reeks.

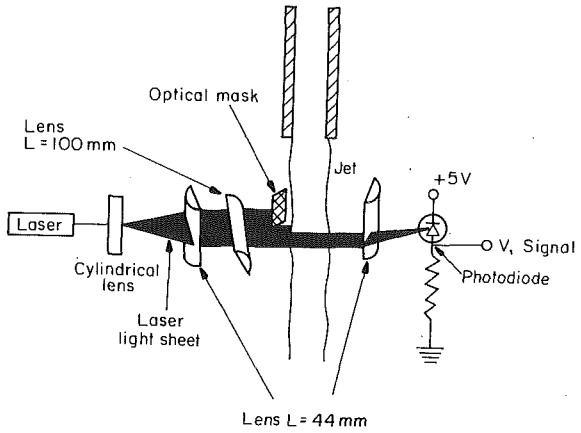

Fig. 1 Optical probe for measuring the instantaneous amplitude of surface disturbances

balance determines the amplitude and evolution of the free-surface disturbances. Here, the high wavenumber (small scale) range of the turbulent pressure spectrum is modeled using results for homogeneous, isotropic turbulence. A force balance between turbulent and capillary pressure is used to calculate the high wavenumber spectrum of the surface disturbances. The theory shows the spectrum to decay as the $-19/3$ power of wavenumber, owing to the capillary damping of the turbulent pressure spectrum. This result is in good agreement with the measured spectra.

2 Experiments

A laser-based optical instrument (Fig. 1) was used to measure the fluctuation amplitudes on the free surface of a turbulent jet in air. A similar instrument was used earlier by Tadrist et al. (1991) to measure the surface disturbances on laminar liquid jets. A 2.4 mW He-Ne laser beam was transformed into a collimated sheet of light by sending it successively through a glass rod and a cylindrical lens (focal length, $L = 44$ mm). This light sheet was further thinned and focused onto the liquid jet by passing it through the axis of a cylindrical lens ($L = 100$ mm) so that an approximately 0.1 mm thick light sheet intersected the jet perpendicular to its axis. A collecting lens ($L = 44$ mm) focused the portion of the light sheet unintercepted by the jet onto a photosensor.

The photosensor was based on an EG&G Vactec photodiode (VTP 8552) and had a dynamic range of about 1 MHz. A 5 Vdc reverse bias was applied to the photodiode, reducing the junction capacitance to 44 pF. The voltage drop across a resistor placed in series with the photodiode provided a signal corresponding to the amount of laser light power incident on the diode. Static calibration showed perfectly linear voltage variation of the measuring system with the width of the intercepted portion of the collimated laser sheet. The rms deviation from linearity was 1 percent of the full scale, i.e., of the voltage reading corresponding to the entire laser sheet. Precise measurements of the diameters of transparent glass rods with this instrument indicated that refraction of light by the object measured has negligible influence on the data. The glass rod (or liquid jet) acts as a diverging lens, and only a negligible portion of the laser sheet is refracted into the direction of the collecting lens. In other words, the jet is effectively an opaque obstruction to the laser sheet.

The output of the photosensor was analyzed by a digital oscilloscope (Hewlett Packard 54200 A/D) and a spectrum analyzer (GenRad 2512A). The oscilloscope provided the true rms voltages over time intervals of the signal. Several such rms voltage outputs were recorded to obtain the rms of the total voltage signal (AC + DC), called V_{tot}, at a given jet axial location. The rms AC component of the signal, V_{ac}, was also recorded at each location. Then, to measure the amplitude of fluctuations at one point on the jet surfce, half of the width of the light sheet incident on the jet was obstructed by an optical mask, so that only the fluctuations from one side of the jet contributed to the fluctuating light power received by the photosensor. The corresponding AC rms signal is denoted by $V_{1/2}$. In addition, the steady voltage signal corresponding to the entire light sheet, *without* any interception by the jet, was obtained as V_0. Owing to the linearity of photodetector response, the ratio of rms amplitude of surface fluctuations to the mean jet diameter[1] can be obtained from these measurements as

$$\frac{\delta_{rms}}{d} = \frac{V_{1/2}}{V_0 - \sqrt{V_{tot}^2 - V_{ac}^2}} \tag{1}$$

The GenRad 2512A spectrum analyzer had a frequency band-

[1]The contraction coefficient for turbulent jets leaving pipe nozzles is essentially unity. Throughout this study, we treat nozzle diameter and initial mean jet diameter interchangeably.

Nomenclature

d = nozzle diameter, m
$F(k)$ = three-dimensional isotropic turbulent pressure spectrum, N^2/m
$G(\eta)$ = power spectrum of the amplitude of free surface disturbances, Eq. 8
k = wavenumber, 1/m
k_1, k_2, k_3 = $j(x, y, z)$ Cartesian components of the wavenumber vector, $k^2 = k_1^2 + k_2^2 + k_3^2$, 1/m
k_p = resultant wavenumber in the (x, y) plane, $\sqrt{k_1^2 + k_2^2}$, 1/m
l = integral scale of turbulence or distance of target from nozzle, m
p = fluctuating component of pressure, N/m^2
t = time, s
u = jet free surface speed, m/s
u_f = jet bulk velocity at the nozzle exit, m/s
u' = rms turbulent speed in liquid, m/s
We_d = jet Weber number, $\rho u_f^2 d/\sigma$
x = distance from the nozzle exit along the jet axis, m
(x, y) = Cartesian coordinates in the plane of the mean liquid surface, m
δ = instantaneous height of the jet surface disturbances, i.e., instantaneous radius minus local mean radius, m
δ^2 = ensemble average of δ^2, m^2
δ_{rms} = rms height of surface disturbances, $\sqrt{(\overline{\delta^2})}$, m
η = dimensionless wavenumber of the free surface disturbances, $l\sqrt{k_1^2 + k_2^2}$
ξ = splattered fraction of incoming jet's liquid
ρ = liquid density, kg/m^3
σ = surface tension between jet liquid and surrounding gas, N/m

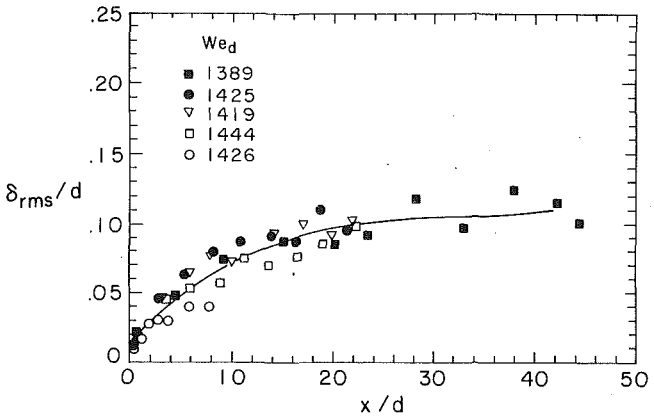

Fig. 2 Variability in repeated measurements of the rms disturbance amplitude: water, $d = 5.8$ mm

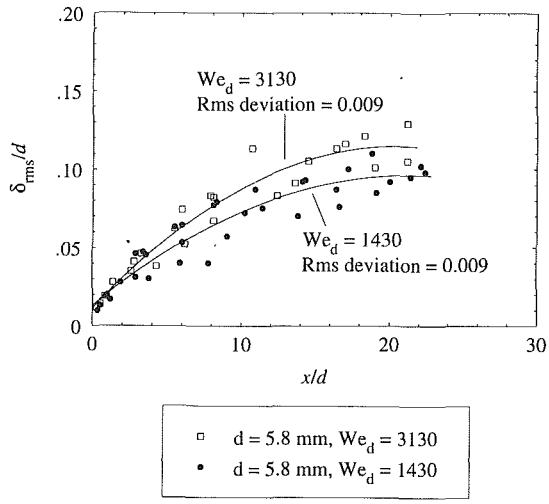

Fig. 3 Measurements of δ_{rms} at two different Weber numbers. For each We_d, a second-order least-squares curve is shown, together with the rms deviation from it

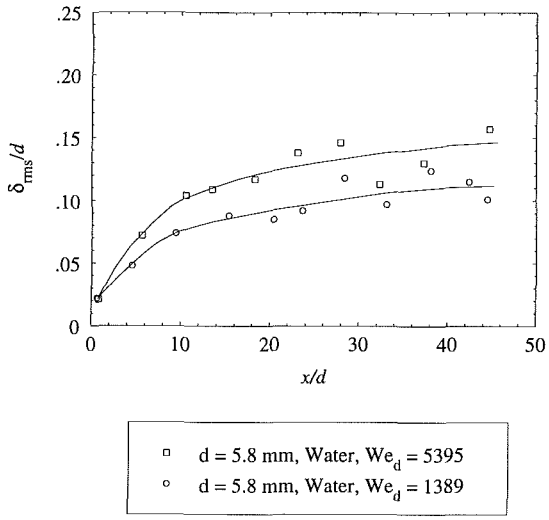

Fig. 4 Measurements of δ_{rms} at two different Weber numbers, with faired curves for each

width of dc to 100 kHz and an amplitude range of 6 decades for the power spectra.

Jets were produced by fully developed turbulent pipe flow from tube nozzles of diameter $d = 2.7 - 5.8$ mm. Measurements were made over the portion of the jet between 0.2 and 45 nozzle diameters downstream of the nozzle. Most experiments were conducted with water; however, for some runs the surface tension was varied by using isopropanol-water mixtures or by using a surfactant detergent. In each case, the surface tension was measured with a ring gauge. Direct measurement of the flow rates (by volume collection) provided the jet Weber numbers with ± 3 percent uncertainty (at 20:1 odds).

Full details of the jet apparatus are given by Bhunia and Lienhard (1994). That study also reports measurements of the fraction of the jet liquid splattered, ξ, during jet impingement on smooth, solid targets under isothermal conditions. As described in that report, the jet Reynolds number has only a very weak influence on the turbulence intensity of jets produced by fully developed pipe flows. Therefore, in the present report, the jet Reynolds numbers are not mentioned, although they can be calculated easily from the nozzle diameters and Weber numbers provided with each data set. The Reynolds number here ranges from 20,000 to 49,000.

Each measurement of δ_{rms} is based on an estimated number of 1000 samples. The actual number of samples varied because of the sampling technique used by the oscilloscope, which reported an rms voltage based on samples that typically had about 100 points. Ten to twelve of the resulting values of δ^2 were averaged to obtain the reported results. Some additional uncertainty can enter into the measurements when the jet Weber number and the length of the jet, x/d, become large enough that droplets are stripped off the jet surface and enter the air flow around the jet. For the measurements reported here, however, this droplet stripping was either absent or of a negligibly low amount.

3 Results of Experiments

Figures 2, 3, and 4 show the rms amplitude of disturbances on turbulent water jets in air. To determine the run-to-run variability of the measurements, several tests were repeated at nearly identical conditions (Fig. 2). The Weber numbers for each test were equal to within the uncertainty limits of ± 3 percent. The rms deviation of the measurements from a second or third order least-squares fit was 0.009, which is about 9 percent of the maximum rms disturbance for this case. The 90 percent confidence intervals of the measurements (according to a chi-squared test of 1000 sample points) are so small that they have essentially the same size as the symbols plotted.

Figure 3 shows the fitted curves for repeated measurements of δ_{rms}/d at two different jet Weber numbers. Although the ranges of variability for the two data sets overlap, the averaged curves show a dependence of the surface disturbance amplitude on the Weber number. This dependence is more pronounced in Fig. 4, which compares jets having a larger difference in Weber numbers.

The amplitudes of disturbances are very small near the nozzle. As the liquid moves downstream, the disturbances grow, but they do not exhibit the exponential increase with x/d that would be expected from Rayleigh's capillary instability theory (Drazin and Reid, 1981; Lienhard et al., 1992). Some consideration of the graphs also shows that the disturbance growth rate parameter predicted by Rayleigh's theory, $(x/d)/\sqrt{We_d}$, cannot correlate the disturbance amplitude data for jets of different diameters and Weber numbers.

Figure 5 compares the surface roughness evolution for liquids of different surface tension. One case represents a mixture of 10 percent by volume isopropanol in water, which has a static surface tension 58 percent lower than pure water (0.042 N/m versus 0.072 N/m). The evolution of δ_{rms} compares favorably with the data for a water jet at the same Weber number and x/d.

Figure 5 also show data for a surfactant-water jet. At rest, the surfactant solution has a surface tension of only 0.027 N/m. Our previous study of splattering (Bhunia and Lienhard,

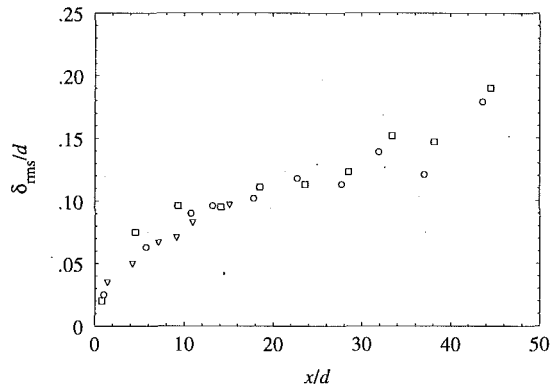

Fig. 5 Comparison of δ_{rms} evolution among liquids with different surface tensions. The Weber number in parentheses is based on pure-water surface tension

1994) showed that surfactants have no effect on splattering behavior: the splattering scaled with a Weber number based on the surface tension of pure water, rather than the surface tension of the static surfactant mixture. From this, it appeared that the turbulent jet surface never achieves a sufficient concentration of surfactant to exhibit a lowered surface tension, either because the diffusion timescales are too long relative to x/u_f or because turbulent free-surface renewal limits the surfactant's surface concentration. Figure 5 supports that conclusion, since the roughness evolution of the surfactant jet is identical to that of a pure water jet having the same size and speed. For those data, the higher Weber number shown is based on the static surface tension, while the lower is based on the surface tension of pure water. The lower value equals that of the pure water jet.

When a turbulent liquid jet impinges onto a solid target, droplets are splattered off the liquid sheet that moves across the target. Figure 6 reproduces measurements of the fraction of incoming jet liquid splattered, ξ, reported earlier (Bhunia and Lienhard, 1994). Near the nozzle ($x/d < 10$, say), ξ changes very little as the jet Weber number varies from 1400 to 7300. Similarly, the variation in δ_{rms}/d with the jet Weber number in Figs. 3 and 4 is also relatively weak near the nozzle. Farther downstream, the dependence on jet Weber number is stronger both for δ_{rms}/d and ξ. These observations suggest a correlation between the two variables, and such a correlation was the basic hypothesis of previous models of splattering (Lienhard et al., 1992). We may now examine this correlation quantitatively.

Figure 7 shows the splatter fraction, ξ, as a function of the rms amplitude of jet surface disturbances. Each point on this graph is obtained by plotting a previously measured splatter fraction ξ (Bhunia and Lienhard, 1994) against δ_{rms}/d from present experiments for jets of same Weber number and $x/d = l/d$. Each set of data for a given nozzle diameter and Weber number consists of measurements at several different axial locations, x/d. The correlation is reasonably clear, given that both δ_{rms} and ξ have significant variability, and this provides further evidence that the jet impingement splattering results from the presence of surface disturbances on turbulent jets and is governed by the amplitude of those disturbances.

For more unusual liquids, various surface-tension phenomena can be expected to alter the surface-roughness evolution and its relation to splattering. For example, surface polymerizing agents (such as are often used to suppress to jet breakup)

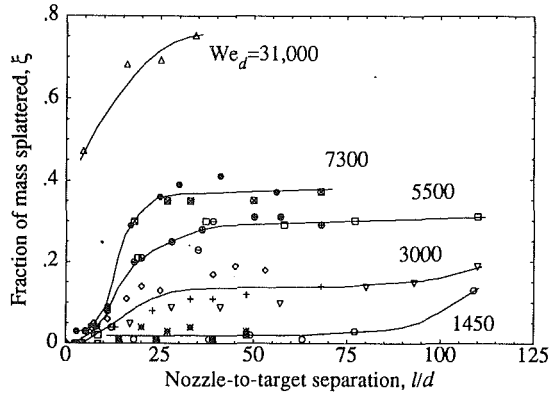

△	d=4.4 mm, Re_d=98097, We_d=31243
⊠	d=4.4 mm, Re_d=48284, We_d=7564
●	d=2.7 mm, Re_d=37141, We_d=7096
⊖	d=5.8 mm, Re_d=47800, We_d=5628
⊕	d=4.4 mm, Re_d=41437, We_d=5420
□	d=2.7 mm, Re_d=31868, We_d=5373
◇	d=5.8 mm, Re_d=35986, We_d=3101
+	d=4.4 mm, Re_d=30090, We_d=2858
▽	d=2.7 mm, Re_d=24580, We_d=3108
✱	d=5.8 mm, Re_d=24507, We_d=1479
■	d=4.4 mm, Re_d=20988, We_d=1430
○	d=2.7 mm, Re_d=16320, We_d=1409

Fig. 6 Splattering as a function of nozzle-to-target separation and jet Weber number. The solid lines are fitted curves through groups of data having We_d constant to within its uncertainty (±3 percent)

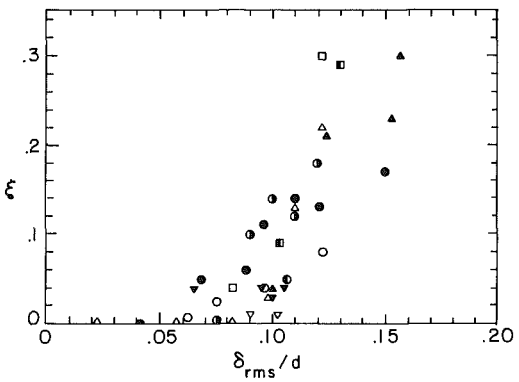

Fluid	d (mm)	We_d
● Isopropanol / Water	5.8	3200
▲ Water	5.8	5500
●		3120
▼		1450
□ Water	4.4	7535
△		5290
○		2850
▽		1400
◧ Water	2.7	7000
◐		3175

Fig. 7 Dependence of the splattering fraction on the rms amplitude of surface disturbances

may be expected to suppress splattering significantly. As another example, long chain alcohols in aqueous solution require a finite time to establish the static surface tension at a freshly formed liquid surface (Addison, 1945), owing to their tendency

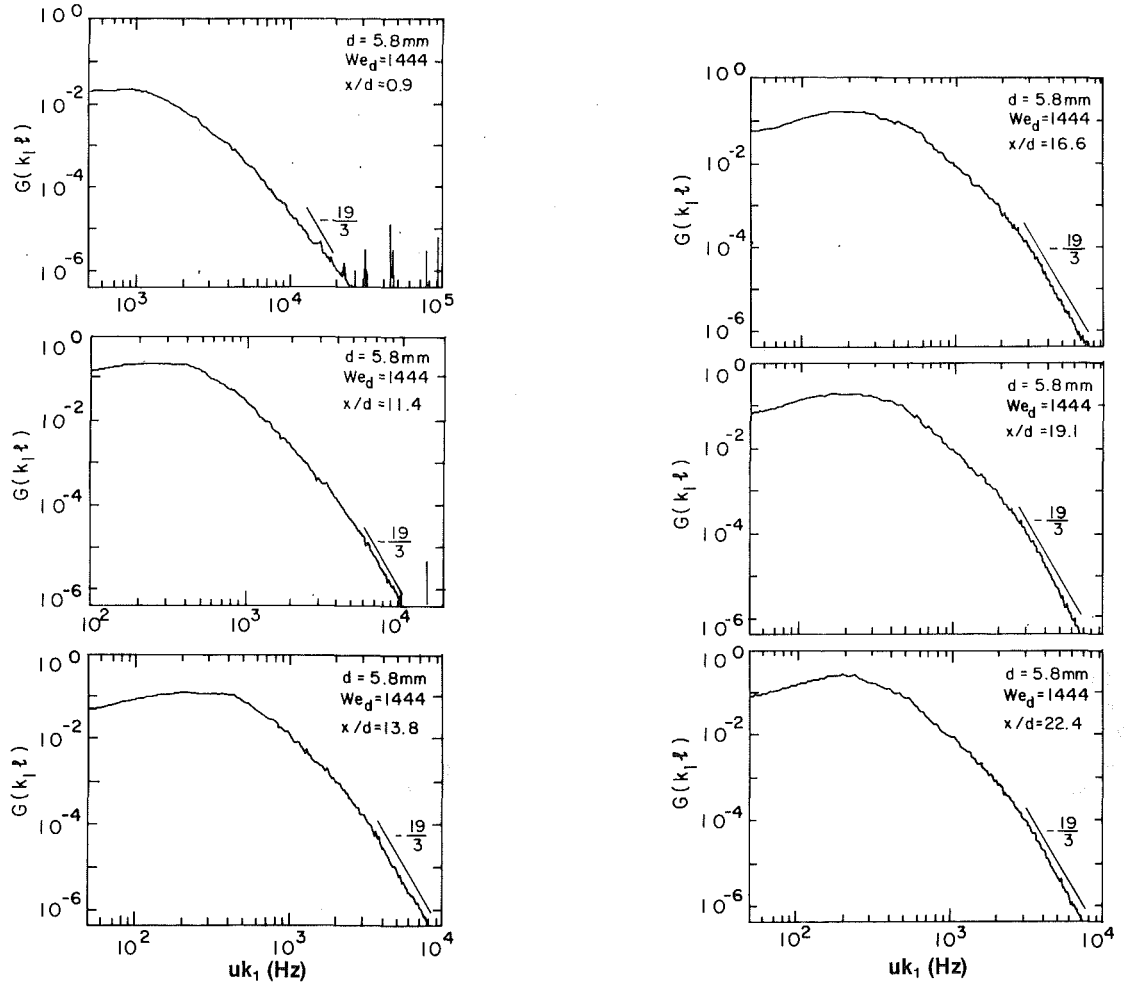

Fig. 8 Measured spectra of free-surface disturbances on a turbulent liquid jet at different axial locations. The ordinate is *proportional* to $G(k_1 l)$

to form a surface monolayer. Thus, for long chain alcohol solutions, a simple Weber number may not effectively scale roughness evolution and splattering, in contradiction to our observations for isopropanol.

3.1 Roughness Spectra. The local distribution of disturbance wavelengths on the jet surface can elucidate the mechanism of surface roughening. Figure 8 shows the spectra of surface-disturbance amplitudes at several different axial locations. The ordinate is proportional to the power spectrum of the free surface disturbance amplitude, $G(k_1 l)$ (see Eq. (8)) and the abscissa is uk_1, where k_1 is the wavenumber in the direction of the jet axis, u is the free surface velocity, and l is the integral scale of turbulence. The spikes at very high frequencies are a reproducible noise signature of the electronics.

These graphs of power spectrum versus disturbance wavenumber show that broad-band turbulent disturbances are more prevalent than any single-wavenumber disturbance related to a Rayleigh-type instability. In the sense of Rayleigh's capillary instability, the low wavenumbers are unstable and the high wavenumbers are stable; the most unstable wavenumber corresponds to $uk_1 = 1017$ Hz. Although this frequency is within the portion of the spectrum that contributes most strongly to the variance of surface roughness (the "knee"), the spectra retain the general appearance of a turbulent cascade from low to high wavenumber. The coupling of the turbulent pressure to the capillary pressure drives the spectral distribution.

These log-log spectral plots show a portion of very nearly linear decrease in the spectral amplitude, characteristic of high wavenumber turbulence. Except for measurement locations very close to the nozzle, the slope of this linear portion is $-19/3$. This novel result is explained in detail in the following section. Similar spectra were obtained for jets of other sizes and the other We$_d$.

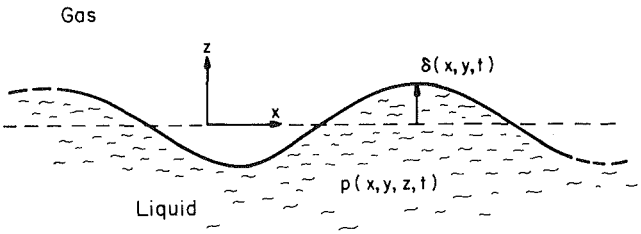

Fig. 9 Geometry of the free surface over a turbulent liquid

4 A Model for Turbulence-Induced Free Surface Disturbances

To examine the relationship between the disturbance spectrum and the pressure spectrum, let us consider a planar free surface of infinite dimensions with a turbulent liquid of infinite depth on one side of it (Fig. 9). A rectangular Cartesian coordinate system is positioned so that the (x, y) plane coincides with the mean location of the free surface and negative values of z lie within the liquid below the surface. Let $\delta(x, y, t)$ be the instantaneous amplitude of small surface disturbances relative to the mean free surface position, and let $p(x, y, z, t)$ be

the fluctuating component of liquid pressure at any location (x, y, z). Since the pressure fluctuations on the free surface are balanced by the surface tension, we have at $z \cong 0$

$$p = -\sigma\left(\frac{\partial^2\delta}{\partial x^2}+\frac{\partial^2\delta}{\partial y^2}\right) \tag{2}$$

Let us define Fourier transforms of δ and p as follow:

$$\delta = \int_{-\infty}^{\infty}\int_{-\infty}^{\infty} \Delta(k_1, k_2, t)e^{-i(k_1x+k_2y)}dk_1dk_2 \tag{3}$$

and

$$p = \int_{-\infty}^{\infty}\int_{-\infty}^{\infty}\int_{-\infty}^{\infty} P(k_1, k_2, k_3\ t)e^{-i(k_1x+k_2y+k_3z)}dk_1dk_2dk_3 \tag{4}$$

Substituting into Eq. (2), we get

$$\int_{-\infty}^{\infty} P(k_1, k_2, k_3, t)dk_3 = \sigma(k_1^2+k_2^2)\Delta(k_1, k_2, t) \tag{5}$$

To describe any time-evolution of the statistical moments of δ and p, the Navier-Stokes equation with proper boundary and initial conditions must be used. In this model, we restrict our attention to the instantaneous statistical relation between p and δ. We suppose the statistics to be taken over spatial intervals large compared to the turbulent integral scales but small compared to the axial distance over which the surface disturbances evolve significantly. In practice, this means wavelengths of a few jet diameters or less. Since the actual measurements are time averages taken at a single spatial location, we are in effect applying the usual Taylor hypothesis (Monin and Yaglom, 1975) to obtain the wavenumber spectrum from the frequency spectrum, with frequency $= uk_1$. Thus, while the statistics of p and δ in the subsequent analysis are instantaneous spatial averages, the measured parameters correspond to time-averages at any spatial location.

Assuming the turbulent pressure fluctuations to be a spatially homogeneous stationary random process, the three-dimensional turbulent pressure spectrum, $F(k)$, can be defined in the usual way by taking a one-point ensemble-average moment of Eq. (4):

$$\overline{p^*p} = \ldots = \int_{-\infty}^{\infty}\int_{-\infty}^{\infty}\int_{-\infty}^{\infty} F(k)dk_1dk_2dk_3 \tag{6}$$

where the * indicates a complex conjugate.[2] Multiplying Eq. (3) by its complex conjugate and ensemble averaging, we obtain with Eqs. (5) and (6)

$$\overline{\delta^2} = \overline{\delta^*\delta} = \int_{-\infty}^{\infty}\int_{-\infty}^{\infty} \frac{1}{\sigma^2(k_1^2+k_2^2)^2}\int_{-\infty}^{\infty} F(k)dk_3dk_2dk_1 \tag{7}$$

For isotropic, homogeneous turbulence (George et al., 1984),

$$F(k) \sim 0.26\rho^2u'^4l^3(kl)^{-13/3},\ kl \gg 1$$

where u' is the rms fluctuating component of turbulent velocity and l is the integral scale of turbulence. Let us define the one-dimensional spectrum of disturbances, $G(\eta)$, by the following equation:

$$\frac{\overline{\delta^2}}{l^2} = \int_0^{\infty} G(\eta)d\eta \tag{8}$$

Here, η is the wavenumber of the free surface disturbances nondimensionalized with the integral scale of turbulence, l. From Eqs. (7) and (8), it follows that at high wavenumbers $(\eta \gg 1)$ the disturbance spectrum is

$$G(\eta) \sim 0.26 \times 2\pi \frac{\rho^2u'^4}{\sigma^2}\frac{l^{-13/3}}{k_p^3}\int_{-\infty}^{\infty}\frac{dk_3}{(k_p^2+k_3^2)^{13/6}} \tag{9}$$

where we have transformed from Cartesian to polar coordinates in the wave number plane $[(k_1, k_2) \rightarrow (k_p, \theta)]$, with $\eta = k_pl$. Upon evaluating the integral, the spectrum of free-surface turbulent disturbances is found to be

$$G(\eta) \sim 2.41\left(\frac{\rho^2u'^4l^2}{\sigma^2}\right)\eta^{-19/3},\ \eta \gg 1 \tag{10}$$

This result explains the observed $-19/3$ slope in the log-log plots of the disturbance spectra as being a consequence of the $k_1^{-7/3}$ variation of the one-dimensional spectrum of the pressure fluctuations (George et al., 1984) and a factor of k_1^{-4} introduced by the derivatives of δ in the capillary force balance equation. It should be noted that this is the *steepest possible slope* for wave numbers less than the Kolmogorov scale. For free surfaces over liquid having a significant mean shear stress, we expect different slopes at high wavenumber, since the corresponding pressure spectra have different slopes (George et al., 1984). For example, in the case of jets, near the nozzle we should see slopes different from $-19/3$ at high wave numbers. These conclusions are each confirmed by the measured spectra (Fig. 8).

The success of this model is due in part to its focus on the high wavenumbers: theoretical and experimental studies of otherwise-homogeneous turbulence near a plane interface show that the higher wavenumbers retain a homogeneous character near the free surface (Hunt and Graham, 1978; Brumley, 1984).

Finally, it is interesting to note that for small amplitudes, the mean increase in jet surface area is proportional to $\int_0^{\infty}\eta^2G(\eta)d\eta$, as can be shown by manipulation of the integral for surface area in terms of $\delta(x, y)$. This implies that the high wavenumber spectrum of the surface-energy increase of the jet is proportional to $\eta^2G(\eta) \sim \eta^{-13/3}$.

5 Conclusions

A nonintrusive optical technique has been used to measure the instantaneous amplitude of surface disturbances on turbulent liquid jets and to study the evolution of rms surface roughness. The spectrum of disturbance amplitudes has also been measured, and a simple theory for its high wavenumber behavior has been developed.

- Measurements show a nonexponential growth of the rms amplitude of jet surface disturbances as the jet travels downstream. The disturbance evolution depends on Weber number and x/d.
- Surface-tension effects on jet roughness scale with the jet Weber number, as demonstrated by comparing results for water jets and isopropanol-water jets. Surfactants have no effect on the roughness, presumably because the surfactant is unable to reach the surface concentration necessary to alter surface tension.
- The amplitude of turbulent jet surface disturbance is correlated with the fraction of liquid splattered during jet impingement.
- The spectra of surface disturbances show that turbulent disturbances dominate over any single-wavelength Rayleigh-type unstable disturbance. The log-log slope of the disturbance spectrum at high wavenumber is $-19/3$. Near the nozzle, the high wavenumber slopes are different owing to alteration of the pressure spectrum by the residual mean shear force in the bulk liquid.
- A mathematical model of free-surface/turbulence interaction is developed. The model predicts the observed $k^{-19/3}$ high wavenumber decay of the disturbance spectrum.

Acknowledgment

This work was supported by the National Science Foundation under grant number CBTE-8858288.

[2]For wavevectors $\vec{k}'$ and $\vec{k}$, $\overline{P^*(\vec{k}')P(\vec{k})} = F(k)\,\delta_{\text{Dirac}}(\vec{k}' - \vec{k})$ if p is a stationary random function.

References

Addison, C. C., 1945, "The Properties of Freshly Formed Surfaces. Part IV. The Influence of Chain Length and Structure on the Static and Dynamic Surface Tensions of Aqueous Alcoholic Solutions," *Journal of Chemical Society*, pp. 98–106.

Bhunia, S. K., and Lienhard V, J. H., 1994, "Splattering During Turbulent Liquid Jet Impingement on Solid Targets," ASME JOURNAL OF FLUIDS ENGINEERING, Vol. 116, No. 2, pp 338–344.

Brumley, B., 1984, "Turbulence Measurements Near the Free Surface in Stirred Grid Experiments," *Gas Transfer at Water Surfaces*, W. Brutsaert and G. H. Jirka, eds., Reidel Publishing Co., pp. 83–92.

Chen, T.-F., and Davis, J. R., 1964, "Disintegration of a Turbulent Water Jet," *J. Hydraulics Division*, Proc. ASCE, HY 1, Jan., pp. 175–206.

Drazin, P. G., and Reid, W. H., 1981, *Hydrodynamic Stability*, Cambridge University Press, Cambridge, UK.

George, W. K., Beuther, P. D., and Arndt, R. E. A., 1984, "Pressure Spectra in Turbulent Free Shear Flows," *Journal of Fluid Mechanics*, Vol. 148, pp. 155–191.

Hoyt, J. W., Taylor, J. J., and Runge, C. D., 1974, "The Structure of Jets of Water and Polymer Solution in Air," *Journal of Fluid Mechanics*, Vol. 63, pp. 635–640.

Hunt, J. C. R., and Graham, J. M. R., 1978, "Free-Stream Turbulence Near Plane Boundaries," *Journal of Fluid Mechanics*, Vol. 84, pp. 209–235.

Kim, S., and Mills, A. F., 1989, "Condensation on Coherent Turbulent Liquid Jets: Part I—Experimental Study," ASME *Journal of Heat Transfer*, Vol. 111, Nov., pp. 1068–1074.

Lienhard V, J. H., Liu, X., and Gabour, L. A., 1992, "Splattering and Heat Transfer During Impingement of a Turbulent Liquid Jet," ASME *Journal of Heat Transfer*, Vol. 114, May, pp. 362–372.

Monin, A. S., and Yaglom, A. M., 1975, *Statistical Fluid Mechanics: Mechanics of Turbulence*, Vol. 2, MIT Press, Cambridge, MA, p. 449.

Tadrist, L., Alaoui, E. K. O., Occelli, R., and Pantaloni, J., 1991, "Experimental Study of a Liquid Jet Flowing Into Another Immiscible Liquid, 'A Local Analysis of the Interface'," *Experiments in Fluids*, Vol. 12, pp. 67–75.